The EMBO Journal vol.14 no.19 pp.4849–4859, 1995

Relative orientation of RNA helices in a group I ribozyme determined by helix extension electron microscopy

Toru M.Nakamura[1], Yuh-Hwa Wang, Arthur J.Zaug[1], Jack D.Griffith[2] and Thomas R.Cech[1,3]

[1]Howard Hughes Medical Institute, Department of Chemistry and Biochemistry, University of Colorado, Boulder, CO 80309 and [2]Lineberger Comprehensive Cancer Center, University of North Carolina, Chapel Hill, NC 27599, USA

T.M.Nakamura and Y.-H.Wang have contributed equally to this work

[3]Corresponding author

The relative orientation of helical elements in a folded RNA molecule provides key information about its three-dimensional architecture. We have developed a method that involves extending peripheral helices of an RNA, mounting for electron microscopy in the absence of protein and measuring interhelical angles. As a control, extended anticodon and acceptor stems of $tRNA^{Phe}$ were found to form a 92 ± 20° angle, consistent with the X-ray structure. Single, double and triple extensions (50–80 bp) of helical elements P2.1, P6b and P8 of the *Tetrahymena* group I ribozyme did not alter its catalytic activity. The measured angle between P6b and P8 is consistent with the Michel–Westhof structural model, while the P2.1–P6b and P2.1–P8 angles allow P2.1 to be positioned in the model. The angle distributions of the ribozyme are broader than those of the tRNA, which may reflect the dynamics of the RNA. Helix extension allows low-resolution electron microscopy to provide much higher resolution information about the disposition of helical elements in RNA. It should be applicable to diverse RNAs and ribonucleoprotein complexes.

Keywords: electron microscopy/group I intron/ribozyme/RNA structure/tRNA

Introduction

Specific folded structures are important for biological activity of many RNAs. RNA base pairing interactions (secondary structure) can be identified with confidence by comparative analysis of functionally equivalent RNAs from phylogenetically diverse organisms (Woese and Pace, 1993) or from populations of RNA selected *in vitro* for a particular function (Gold *et al.*, 1993). Three-dimensional (3-D) RNA structures, on the other hand, have been determined at atomic resolution for only a handful of biological RNAs (Kim *et al.*, 1974; Robertus *et al.*, 1974; Pley *et al.*, 1994) and small RNA motifs (Wyatt and Tinoco, 1993). Transfer RNAs remain the largest RNAs for which 3-D structures have been solved at X-ray crystallographic resolution.

The approximate 3-D structural organization of RNAs can be probed by experimental methods such as cross-linking (Wang *et al.*, 1993; Harris *et al.*, 1994), chemical modification/protection assays (Latham and Cech, 1989; Moazed and Noller, 1989; Wang and Cech, 1992), fluorescence energy transfer (Tuschl *et al.*, 1994) and transient electric birefringence (Amiri and Hagerman, 1994; Shen and Hagerman, 1994; Friederich *et al.*, 1995). Such experimental data, together with phylogenetic data, have been used to develop 3-D models of several large RNAs, including 5S and 16S rRNA, the RNA subunit of ribonuclease P, the catalytic core of group I self-splicing introns and the hepatitis delta ribozyme (Brimacombe *et al.*, 1988; Stern *et al.*, 1988; Westhof *et al.*, 1989; Michel and Westhof, 1990; Harris *et al.*, 1994; Malhotra and Harvey, 1994; Tanner *et al.*, 1994; Westhof and Altman, 1994). Despite their limited resolution, these models provide useful frameworks for designing further experiments and have helped researchers understand how RNAs might carry out their tasks in 3-D.

The special advantage of ribozymes for studies of RNA structure is that they report their conformation through the reactions they catalyze. The L-21 Sca I ribozyme used in this study is a 388 base derivative of the self-splicing group I intron of *Tetrahymena thermophila* pre-rRNA. It catalyzes the site-specific endonucleolytic cleavage of an RNA substrate by an intron-bound guanosine nucleophile, a reaction analogous to the first step of splicing (reviewed in Cech, 1990; Cech *et al.*, 1992; Cech, 1993). The secondary structure of the *Tetrahymena* ribozyme has been well established by phylogenetic methods (Michel and Dujon, 1983; Waring *et al.*, 1983; Michel and Westhof, 1990) and numerous mutagenesis studies. The 3-D organization of its catalytic core has been modeled by Michel and Westhof (1990) and several aspects of the model (the active site geometry around the P1 helix and the guanosine binding site in P7) have since been supported by experiments involving affinity cleavage by a substrate analog, site-specific photocross-linking and the combination of genetic and biochemical analyses (Pyle *et al.*, 1992; Wang and Cech, 1992; Wang *et al.*, 1993). However, even the model of the core has few experimentally validated constraints, and regions outside of the core have not yet been modeled.

In this paper we report the development of an experimental approach that uses electron microscopy (EM) to map the 3-D organization of RNA molecules. We have previously shown by EM that the L-21 Sca I ribozyme forms a compact, globular structure with 116 (±14) Å diameter in the presence of Mg^{2+} ions (Wang *et al.*, 1994). Transmission electron microscopy, however, has insufficient resolution to show the specific location or orientation of structural elements within the ribozyme. To determine the relative orientation of RNA helices, we have taken advantage of the lack of length constraints of

many peripheral helical elements of group I introns. Helical insertions were made at the ends of several stem–loop structures of the ribozyme, and catalytic activity of these altered ribozymes was measured to make sure that the extensions did not cause any discernible misfolding. The extended helices can be directly seen by EM and the angles between pairs of extended helices were measured to obtain information about the geometry within the ribozyme. Our data support and extend the Michel–Westhof core model. We discuss the possibility that the distribution of measured angles reflects the intrinsic dynamics of the RNA in solution, information which cannot be obtained from many of the methods that average a population of molecules. This method should be applicable to studies of the 3-D organization of a wide variety of structured RNA molecules.

Results

tRNA structure analysis by EM

We first wished to establish that extended helices are visible by EM and that the angles observed between two extended helices actually reflect the native tertiary folding of the RNA. For this purpose yeast $tRNA^{Phe}$ with ~70 bp extensions of the anticodon and acceptor stems (Friederich *et al.*, 1995) was mounted for EM in the presence of Mg^{2+}. Individual tRNA molecules could be easily seen as 'L' shaped structures (Figure 1A). The angle between the two extended arms showed a sharp peak around 90–100° (Figure 1B), consistent with the predicted angle of ~90° from the crystal structure (Kim *et al.*, 1974; Robertus *et al.*, 1974) and the measurement of 89 ± 4° by transient electric birefringence (Friederich *et al.*, 1995). Measurements from an independent EM experiment showed excellent reproducibility of the angular distribution (Table I). These results indicate that the mean or median angle observed between two extended helices by EM correctly reports the angle in the native RNA. The standard deviation of the angle measurements was ±20°, significantly greater than the measurement error (total range of ±5°, based on multiple measurements of the same molecule).

Design and construction of the ribozymes with extended helices

Five stem–loops in the secondary structure of the L-21 Sca I ribozyme were selected for helix extension: P1, P2.1, P6b, P8 and P9.2 (Figure 2). Extension of these helices was judged unlikely to perturb the RNA tertiary structure by the following criteria: (i) they were accessible to free radical cleavage by Fe(II)–EDTA (Latham and Cech, 1989) and therefore likely to be on the surface of the folded RNA; and (ii) results of phylogenetic and mutational analysis have suggested that the size or identity of bases at the ends of these helices is not essential for catalytic activity of the ribozyme. For example, long open reading frames (ORFs) interrupt the ends of P1, P6b and P8 helices in several group I introns (Damberger and Gutell, 1994). Furthermore, previous deletion studies showed that P6b can be truncated without changing splicing activity (Price *et al.*, 1985) and that nucleotides following the *Nhe*I site at position 355, which include elements P9.1 and P9.2, are not required for the first step

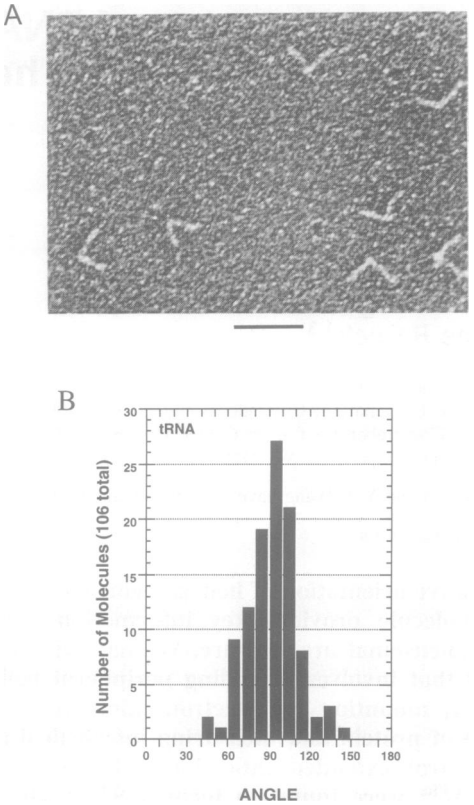

Fig. 1. The $tRNA^{Phe}$ extension control. (**A**) Electron microscopic visualization of the heteroduplex tRNA molecule in which the anticodon and acceptor stems have each been extended by ~70 bp (Friederich *et al.*, 1995). Micrograph is shown in reverse contrast. The bar represents 500 Å. (**B**) Angular distribution between extended helices of the tRNA.

of splicing (Szostak, 1986). Although the P9.2 extensions were not examined by EM in the present work, their construction and activity are reported here for those interested in the effects of helix extension on ribozyme activity.

To insure visibility by EM, ribozyme helices P1, P2.1 and P9.2 were extended by ~50 bp and helices P6b and P8 by ~80 bp. Due to the long palindromic sequences created by extension, direct cloning of the DNA encoding an entire helix extension into one plasmid was not feasible. When a ligation reaction was used to transform *E.coli*, we were never able to recover the plasmid that contained ligated palindromic inserts. We suspect this was due to instability of the palindromic sequence in *E.coli* (Collins, 1980; Lilley, 1981).

Therefore, we decided to clone the 5′ and 3′ halves of each extension into separate plasmids. For example, for the P6b + P8 extension ribozyme, the DNA template was cloned as three separate pieces representing the 5′ end of the ribozyme through the 5′ half of the P6b extension, the 3′ half of the P6b extension through the 5′ half of the P8 extension, and the 3′ half of the P8 extension through the 3′ end of the ribozyme (Figure 3). These extensions were introduced by long PCR primers, each of which contained an annealing region (~25 nt), the extension sequence (~50 or 80 nt) and restriction enzyme site(s) for cloning (see Figure 3A for locations and orientations of DNA primers used in this study). Correct size PCR products were then ligated into plasmids and cloned, and

Table I. Summary of angular distributions observed by EM

RNA	Product oligo[a]	Experiment	No. of molecules	Mean ± SD	Median
tRNA	NA	1	124	92 ± 21	92
	NA	2	106	93 ± 18	94
P2.1 + P6b	+	1	105	86 ± 39	74
	+	2	140	75 ± 35	66
	−	1	102	85 ± 37	80
	−	2	108	85 ± 35	81
P2.1 + P8	+	1	82	74 ± 29	71
	+	2	120	76 ± 27	69
	−	1	102	86 ± 29	86
	−	2	126	83 ± 29	83
P6b + P8	+	1	100	95 ± 31	94
	+	2	107	90 ± 33	90
	+	3	111	97 ± 34	97
	+	4	102	93 ± 30	94
	−	1	122	85 ± 36	79
	−	2	132	91 ± 38	90
cis-P1 + P2.1	+	1	118	81 ± 36	76
	+	2	125	82 ± 34	81
cis-P1+ P6b	+	1	139	132 ± 43	133

[a]+, 18 nM ribozyme and 190 nM product oligo. –, only ribozyme.
For the ribozyme that included the *cis*-P1 extension, product oligo was added to keep the P1 helix formed in case cleavage at the 5′ splice site occurred by hydrolysis during preparation. NA, not applicable.

the inserts were sequenced from both directions. To produce a template for a desired extended ribozyme construct these inserts were digested by appropriate restriction enzymes, purified on agarose gels, ligated and amplified by PCR (Figure 3B). The template was then gel purified and transcribed by T7 RNA polymerase. Other extensions were produced in a similar manner (see Materials and methods).

Kinetic analysis of the extended ribozymes

The structural integrity of the helix-extended ribozymes was assessed by measuring their kinetics of site-specific cleavage (Zaug *et al.*, 1986) of an oligoribonucleotide substrate, CCCUCU/AAAAA (where the solidus represents the site of cleavage). The two rate constants determined were $(k_{cat}/K_m)^S$, which for the wild-type ribozyme is rate-limited by RNA substrate binding, and $(k_{cat}/K_m)^G$, which for the wild-type ribozyme is rate-limited by the chemical step of substrate cleavage (Herschlag and Cech, 1990; Figure 4). For the P2.1, P6b, P8 and P9.2 extensions, both kinetic parameters were indistinguishable from those of the wild-type L-21 Sca I ribozyme (Table II). These kinetic parameters are very sensitive to structural perturbations caused by single-base changes within the catalytic core (e.g. Pyle *et al.*, 1992). Therefore, we conclude that these helix extensions are not likely to have affected the overall native 3-D structure of the ribozyme. [The assumption is that ribozymes active under conditions of the activity assay will also be active under EM sample preparation conditions. The EM sample preparation is a non-equilibrium process during which counterions are diluted, so we are not able to assess activity under exactly these conditions. However, our previous studies (Murphy *et al.*, 1994; Wang *et al.*, 1994) have shown that the EM conditions are sufficient to stabilize the 3-D structure of the P4–P6 domain and are sensitive to mutations which destabilize the structure; the starting condition of 70 mM $MgCl_2$ used in the EM sample preparation provides stabilization equivalent to ~10 mM $MgCl_2$ in solution.]

For the constructs containing the *cis*-P1 extension (i.e. P1 was intramolecular) the rates of the cleavage reaction had to be measured in a completely different way, since the reaction site is within P1 (see Figure 2, *cis*-P1 extension). The method involved 5′ end-labeling the extended RNA during *in vitro* transcription in the presence of γ-^{32}P-GTP, and then monitoring the release of the 5′ exon (^{32}P-GGCCCUCU). When this intramolecular scission reaction was measured only a very small fraction (<8%) of the molecules reacted at a fast rate, and the remainder reacted very slowly (10^{-3}–10^{-4} min^{-1}) at 200 μM guanosine (data not shown). The slow rate is unlikely to reflect any defect in the catalytic core, because the *trans*-P1 extension ribozyme was fully active with the short oligonucleotide substrate. Instead it might reflect a problem with docking the extended P1 helix into the active site. Thus the angle measurements of ribozymes containing P1 extensions need to be interpreted with caution, as the majority of RNA on the EM grid has to be in an active conformation for the observed angles to be meaningful. Although we report the angular distribution of *cis*-P1 + P2.1 and *cis*-P1 + P6b in the next section, since these angles might represent the geometry of the ribozyme with P1 undocked, they will be excluded from consideration in our model of the active structure of the ribozyme.

Angular distributions for extended ribozyme helices

When observed in the EM, ribozymes with 0, 1 or 2 extended helices could be clearly differentiated (Figure 5). The globular core was also visible and served as a reference point to assign the direction of measurement (i.e. 90° could be differentiated from 270°). This was in contrast to the extended tRNA molecules, which appeared as two intersecting rods without a visible core.

Histograms showing the angular distributions of doubly-extended ribozymes are shown in Figure 6. In the absence of the reaction product CCCUCU the P1 helix is not formed. These ribozymes showed very broad angular

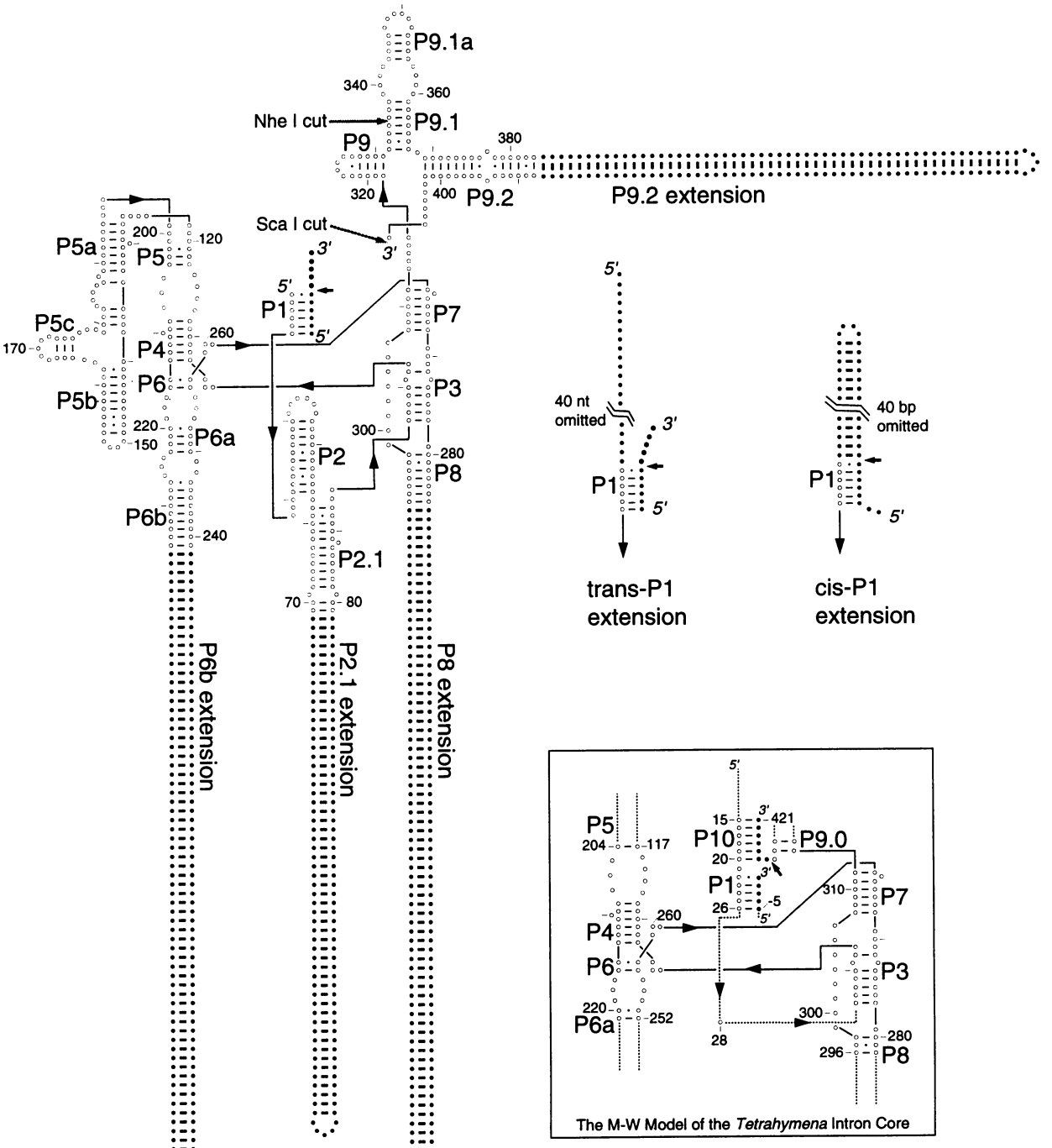

Fig. 2. Secondary structure representation of the L-21 Sca I ribozyme (Cech *et al.*, 1994) with extensions. Open circles represent nucleotides that are present in the wt ribozyme or intron. Filled circles represent either extended nucleotides, RNA substrate (5′-CCCUCUAAAAA-3′) or exon sequences. Arrowheads on connecting lines represent 5′- to -3′ directionality. Small arrow in P1 represents site of cleavage by guanosine. Sizes of ribozymes used in this study: L-21 Sca I ribozyme, 388 nt; *trans*-P1 extension, 448 nt; *cis*-P1 extension, 504 nt; P2.1 extension, 496 nt; P6b extension, 545 nt; P8 extension, 548 nt; P9.2 extension, 495 nt; *cis*-P1 + P2.1 extensions, 612 nt; *cis*-P1 + P6b extensions, 661 nt; P2.1 + P6b extensions, 653 nt; P2.1 + P8 extensions, 656 nt; P6b + P8 extensions, 704 nt; P2.1 + P6b + P8 extensions, 812 nt. Insert shows the portion modeled by Michel and Westhof (1990); dotted lines represent parts of the intron that were not modeled. Small arrow between P10 and P9.0 represents site of exon ligation (the 3′ splice site).

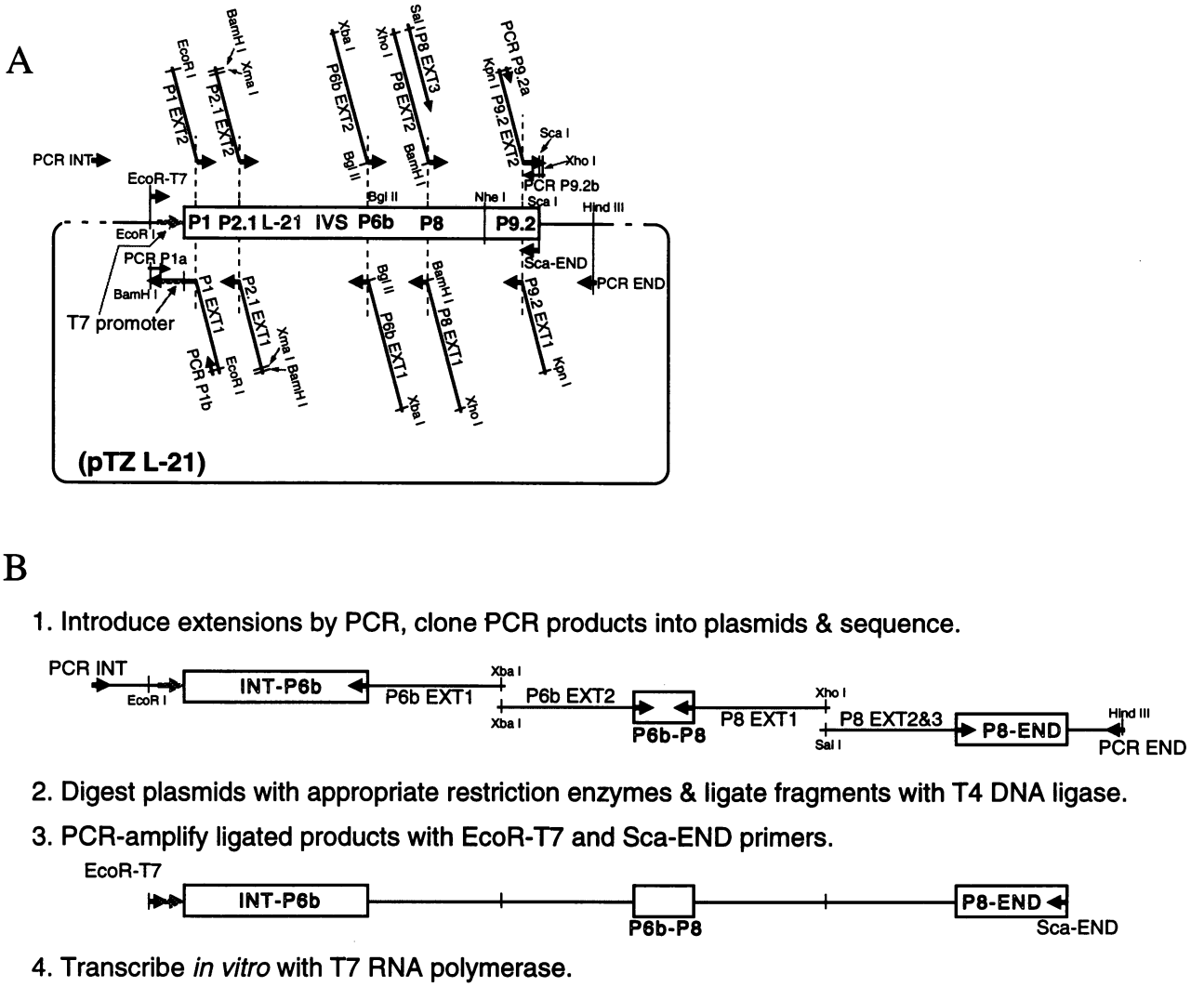

Fig. 3. Strategy used to introduce extensions into the L-21 Sca I ribozyme. (**A**) Schematic diagram of the orientation of PCR primers. For extension primers, horizontal arrows represent annealing sequence and diagonal lines represent extension sequences. Arrows show 5′ to 3′ direction. (**B**) Outline of the construction of the P6b + P8 extension RNA.

distributions (bottom row of Figure 6). When this oligonucleotide was added at a concentration sufficient to form P1, the distributions sharpened (top row of Figure 6); the decrease in breadth was greatest in the case of P6b + P8. This suggests that the RNA structure becomes either more uniform or less flexible when the P1 helix is intact. Interestingly, this sharpening was not reflected in a change in the standard deviation (Table I), which is heavily influenced by the small number of measurements which are far from the mean.

The measured angles were very reproducible between independent experiments. For example, in four trials with the P6b + P8 extended ribozyme, the mean angle ranged from 90 to 97°, and the median also ranged from 90 to 97° (Table I). This reproducibility allows the conclusion that the angle between P6b and P8 is significantly greater than that between P2.1 and P6b or between P2.1 and P8, both of which were in the 70–80° range.

The measured angles between the three pairs of extended helices led to a model of the relative orientation of these helices in the native ribozyme (see Discussion). An independent test of the model involved extending all three helices simultaneously. As shown in Figure 7, the three extended helices could be clearly discerned. The most common helix distribution was for all three arms to lie within a sector of ~90°, and in almost all cases the three arms were within a ~180° sector. Because we could not identify the individual helices we did not attempt to measure the helix angles.

The distributions involving an extended P1 helix are shown in Figure 8. Although these constructed ribozymes contained an intact P1 helix, the product oligonucleotide was still added in case ribozyme-catalyzed cleavage released the product from some of the RNA during preparation, causing a mixed population of ribozyme with product bound and unbound. The doubly-extended *cis*-P1 + P6b construct showed an indication of a bimodal angle distribution. This was reproduced in a second independent EM preparation. This ribozyme construct was the only one with a mean angle significantly >90°; its mean

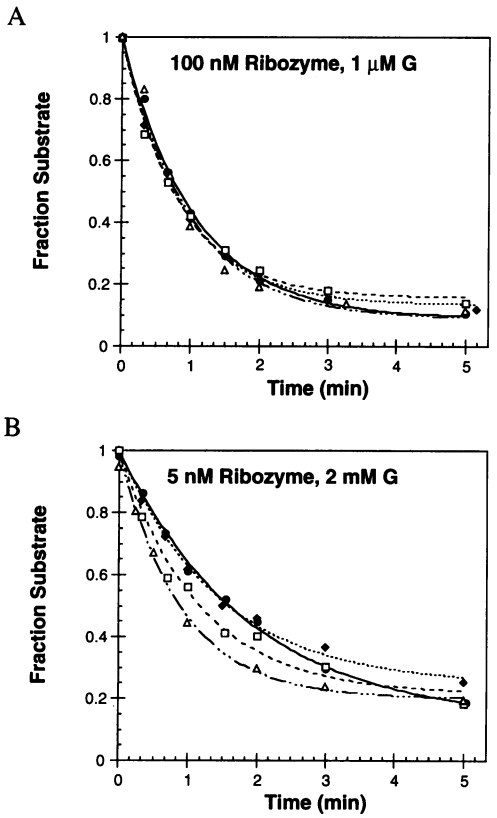

Fig. 4. Sample data for kinetic analysis of helix-extended ribozymes. (**A**) Measurement of $(k_{cat}/K_m)^G$. (**B**) Measurement of $(k_{cat}/K_m)^S$. ●, wt L-21 Sca I; ◆, P2.1 + P6b; □, P2.1 + P8; △, P6b + P8. Lines represent best fits to a single exponential, with a residual fraction of unreactive material that was typically 0.1–0.2.

Table II. Single turnover kinetic parameters for $CCCUCUA_5$ cleavage by extended ribzymes[a]

Ribozyme	$(k_{cat}/K_m)^G$ 10^5 M^{-1} min^{-1}	$(k_{cat}/K_m)^S$ 10^8 M^{-1} min^{-1}
wt	8.5 ± 0.5	1.6 ± 0.5
trans-P1	5.9 ± 2	1.2 ± 2
P2.1	13 ± 2	1.1 ± 0.1
P6b	6.2 ± 0.9	1.4 ± 0.5
P8	8.0 ± 1	1.6 ± 0.3
P9.2	9.9 ± 0.8	0.7 ± 0.4
P2.1 + P6b	9.1 ± 4	1.2 ± 0.4
P2.1 + P8	8.9 ± 4	1.7 ± 0.8
P6b + P8	5.4 ± 3	1.0 ± 0.7
P2.1 + P6b + P8	10 ± 5	1.1 ± 0.9

[a]Each value is the average of two to seven independent measurements. Errors represent standard deviations of measurements.

was 132°, and some of the individual molecules had angles >180°.

Why broad distributions?

It seemed possible that the breadth of the helix angle distributions could be due to random orientation of the molecules on the EM grid. For example, consider two line segments that form a 90° angle. When observed from all possible orientations in three dimensions, the angle will appear to vary from 0 to 180°, and will appear as 90° only when viewed orthogonal to the plane defined by its two line segments. Thus, if the two extended 'arms' of a ribozyme lie flat on the grid, the observed interhelix angle will equal the true angle, whereas if one or both 'arms' extend up or down from the plane of the grid the interhelix angle will be measured as a broader distribution including angles that are both more acute and more obtuse than the true angle.

A test of this possibility involves measuring the length of the two line segments (extended helices). Two line segments that form an angle will appear as full-length only when viewed orthogonal to the plane. If one or both of the line segments is extending towards or away from the viewer, it will appear shorter than full-length. To perform this test, we measured the combined arm lengths of 139 molecules with extended P1 + P6b helices (chosen because this molecule had as broad an angle distribution as any). The angular distributions of the molecules shorter than the mean and those longer than the mean were tabulated separately. In addition, the angular distribution of the molecules closest to the mean arm length (within ±1 standard deviation of the mean) was tabulated. All three of these arm length-selected angle distributions looked very similar to that of the entire set of 139 molecules (data not shown). The distributions did not become sharper, nor did the mean angle change significantly.

Thus, we found no evidence for the angle distributions being broadened by the helices being out-of-plane and therefore viewed through variable angles. Our operating hypothesis is that most of the RNA molecules have their extended helices lying flat on the surface of the EM grid. The breadth of the length distribution is therefore thought to reflect intrinsic flexibility of the molecules and random distortion upon adsorption onto the grid surface, with a small contribution from measurement error (see Discussion).

Discussion

The relative disposition of helical elements in an RNA molecule is the most revealing information for understanding its 3-D architecture. A number of approaches utilize the extension of helical elements to amplify the information about how helices are arranged in the native molecule. These include fluorescence resonance energy transfer (Tuschl *et al.*, 1994), native gel electrophoresis (Bhattacharyya *et al.*, 1990; Amiri and Hagerman, 1994; Shen and Hagerman, 1994; Bassi *et al.*, 1995) and transient electric birefringence (Amiri and Hagerman, 1994; Shen and Hagerman, 1994).

In the current paper we have explored electron microscopic visualization of helix-extended RNA as a direct method for determining the arrangement of helices. Helix extension electron microscopy was validated by angle measurements of tRNA with extended anticodon and amino acyl acceptor stems. It was then applied to the group I ribozyme from *Tetrahymena*, where it gave data consistent with one of the predictions of the current 3-D model (Michel and Westhof, 1990) and some new information about the disposition of one of the unmodeled helices, P2.1.

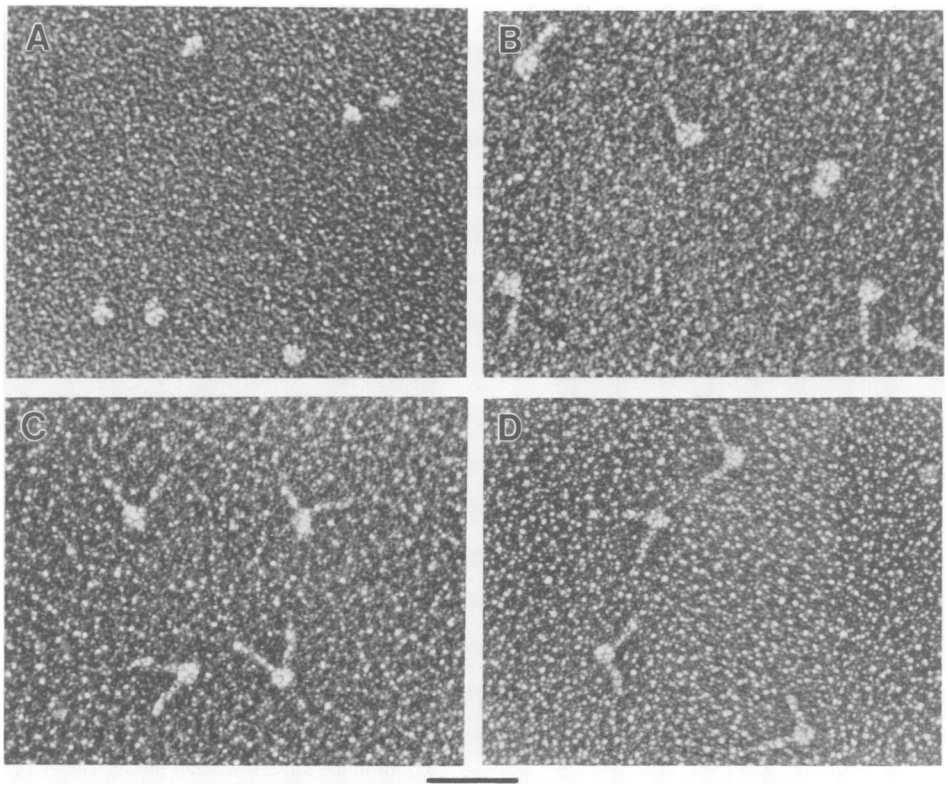

Fig. 5. Electron microscopic visualization of ribozyme constructs. (**A**) wt L-21 Sca I. (**B**) P8 extension. (**C** and **D**) P6b + P8 extension. For (A–C), ribozyme RNA plus product oligo RNA (5′-CCCUCU-3′). For (D), ribozyme alone. Micrographs are shown in reverse contrast. The bar represents 500 Å.

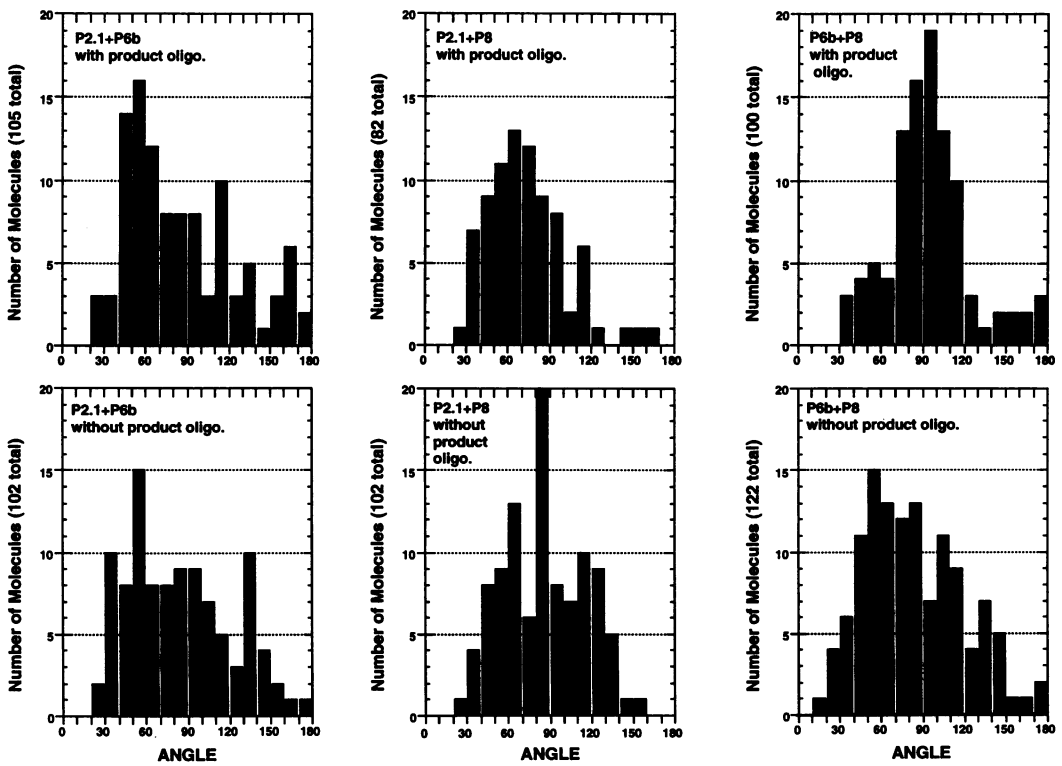

Fig. 6. Distributions of angles between extended helices for P2.1 + P6b, P2.1 + P8 and P6b + P8 extension ribozymes. Top row, ribozyme plus product oligo RNA. Bottom row, ribozyme alone.

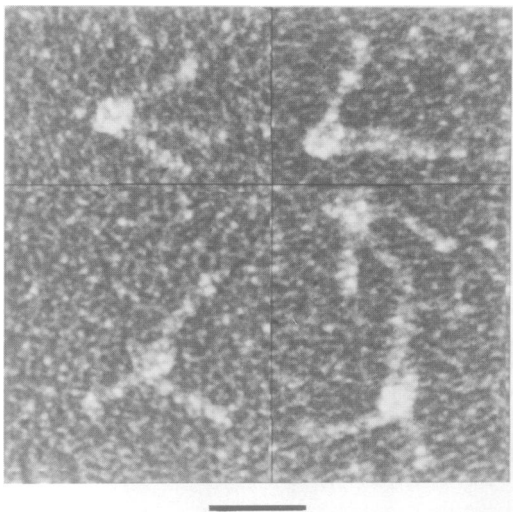

Fig. 7. Electron micrographs of ribozymes with three helices extended (P2.1 + P6b + P8). Sample also contained product oligo RNA. In some cases, the shorter P2.1 extension (~50 bp) can be differentiated from the longer P6 and P8 extensions (~80 bp). The bar represents 200 Å.

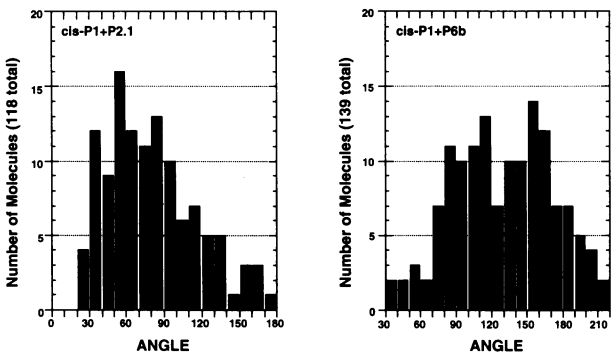

Fig. 8. Distribution of angles between extended helices for *cis*-P1 + P2.1 and *cis*-P1 + P6b ribozymes. Ribozyme plus product oligo RNA. For *cis*-P1 + P6b extension, the position of the globular core was used as the reference point to determine which direction to measure each angle. This was necessary because the angles between P1 and P6b were wide, and in the absence of a reference point all angles >180° would have been measured in the opposite direction (i.e. 180 + *n* would have been counted as 180 – *n*).

Tetrahymena ribozyme

Helical elements P6b and P8 reside in two different domains of the group I ribozyme (Figure 2). Thus, there is no basis for predicting their relative angle without some information about higher-order structure. Michel and Westhof (1990) have combined information from comparative sequence analysis with stereochemical constraints to model the catalytic core of the *Tetrahymena* ribozyme. Several long-range contacts or spatial proximities determined experimentally are in agreement with the model (Pyle *et al.*, 1992; Wang and Cech, 1992; Wang *et al.*, 1993), and there has been one test of a more general architectural feature: the coaxial stacking of P4 and P6 (Murphy *et al.*, 1994).

The Michel–Westhof model includes the proximal portions of the P6a and P8 helices, but not P6b. In the representation shown in Figure 9, both the P6a (blue) and the P8 (yellow) helices have been extended as regular A-form helices. When the coordinates of the two helices

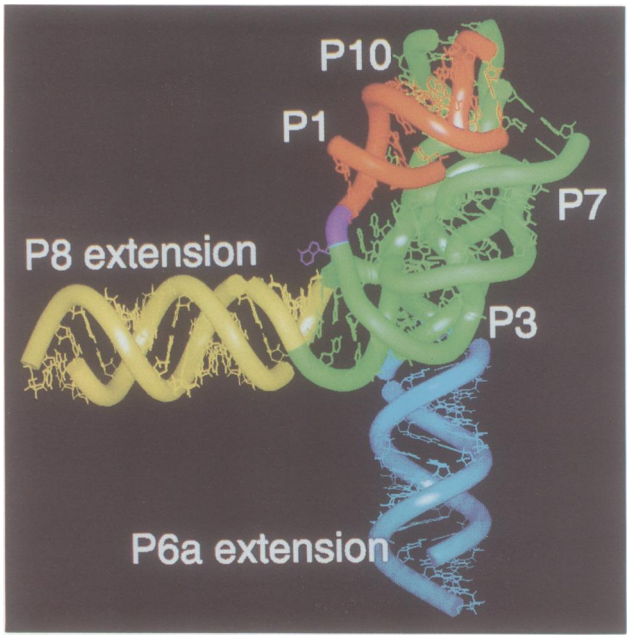

Fig. 9. Estimation of the angle between P6a and P8 helices based on the Michel–Westhof model of the *Tetrahymena* intron core (Michel and Westhof, 1990). A-form RNA duplexes (15 bp each) were added to the ends of the P6a helix (U221–A252) and the P8 helix (G282–C296) in the Michel–Westhof model. The P6a extension is shown in blue and the P8 extension is shown in yellow. P1 and P10 are shown in red, A28 in purple and the rest of the intron core RNA in green. Generated with InsightII (Biosym).

are converted to vectors and their dot product calculated, they are found to form an angle of 96°. This is in excellent agreement with the values obtained from helix extension EM, which were in the 90–100° range (Table I). Note, however, that our crude modeling assumes that P6a and P6b are coaxial; given that they are separated by an asymmetric internal loop, it seems quite possible that P6b would be displaced from the axis defined by P6a. Thus, we do not expect exact agreement between the axis of P6a in the Michel–Westhof model and the axis of P6b determined by electron microscopy when both are measured relative to P8.

The P2 and P2.1 helices are the major structural elements connecting the reaction-site helix (P1) with the catalytic core of the ribozyme (Figure 2). Their positions were not modeled by Michel and Westhof (see insert in Figure 2). We found that the P2.1 helix forms an acute angle with both P6b and P8, suggesting that it protrudes from the approximate plane defined by P6b and P8. Two models fit our data (Figure 10). They are mirror images of each other, and cannot be differentiated by pairwise angle measurements. This orientation of P2.1 differs from that proposed by Downs and Cech (1990); however, this earlier suggestion was based on a model of the catalytic core that preceded the Michel–Westhof model.

As a test of this model, ribozymes were constructed with all three helices extended. Electron microscopic examination (Figure 7) showed a preponderance of molecules with a clustered distribution of the three extended helices, as expected from our model. Quantitation of such angles promises to be problematic, and has not been attempted; if our hypothesis about the two-armed molecules tending to lie flat on the grid is correct then the three-

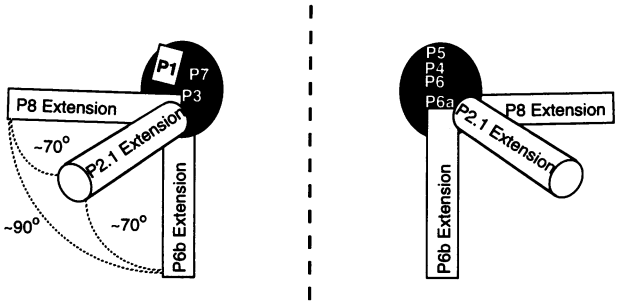

Fig. 10. Model that explains the angles observed for pairwise extensions of the P2.1, P6b and P8 helices of the L-21 Sca I ribozyme with bound oligonucleotide product. Two stereoisomers are consistent with our observations.

armed molecules will presumably have one arm out-of-plane and therefore give apparent angles that do not represent the true angles.

Do widths of angle distributions reflect RNA dynamics?

The most discrete angle distributions we measured were with the helix-extended tRNA (Figure 1B). Because the ±20° width of the angular distribution is so much greater than the ±5° measurement error, we infer that the width represents the flexibility of the molecule in solution, or distortion upon adsorption to the EM grid surface or both. If there is distortion upon adsorption, it must be largely random because the mean angle was so close to that expected for tRNA.

In the case of the helix-extended ribozyme, the distributions were all broader than those of the tRNA. The standard deviation was 28° for P2.1 + P8, 32° for P6b + P8, 35° for *cis*-P1 + P2.1 and 37° for P2.1 + P6b (Table I). The possibility that the breadth was caused by viewing the helices from different angles was tested in one case, and found not to pertain (see Results). We therefore suggest that the ribozyme helices are held into place less rigidly than those of tRNA, or else are more subject to distortion upon mounting onto the EM grid. The *cis*-P1 + P6 RNA consistently showed a broad, biphasic distribution. This suggests that the population was structurally heterogeneous, and indeed it was found to be heterogeneous in terms of its activity.

The broader angle distributions of the ribozyme relative to tRNA correlate with the domain structures of these RNAs. In the ribozyme, P6b is in a domain separate from P8 and P2.1 (Murphy and Cech, 1993, 1994), and it is reasonable that there would be more flexibility between domains than within the single-domain tRNA. The relationship of P2.1 to the domain structure of the ribozyme has not been established, so we have no basis for predicting widths of angle distributions that include an extended P2.1. Based on our data, P2.1 seems to be more tightly associated with the domain containing P8 (±28° width) than with the domain containing P6b (±37° width).

Each of the angular distributions sharpened when the ribozyme was bound to its reaction product oligonucleotide prior to EM. This is consistent with the hypothesis that the breadth of the angle distribution reflects the flexibility of the RNA in solution, and that the structure tightens up upon formation of the P1 reaction site helix.

Applications

Helix extension electron microscopy should be useful for determining relative angles between helical elements in other ribozymes and ordered RNA molecules in general. Furthermore, many RNAs including *Neurospora* mitochondrial group I introns, the yeast bI5 mitochondrial intron, RNase P, small nuclear RNAs and ribosomal RNAs are active as ribonucleoprotein complexes, so the effect of the protein cofactor on the disposition of RNA helices could be determined.

Materials and methods

Construction of extended tRNA^{Phe}

Plasmids pGJ122A9 and pGJ122B11 were obtained from P.J.Hagerman's group (Friederich *et al.*, 1995). They encoded the 5′ half (nt 1–31) and 3′ half (nt 39–72) of yeast tRNA^{Phe}, respectively. Each tRNA half was bounded by extensions that were complementary to each other. Plasmids were linearized by *Sma*I digest, transcribed and then gel purified essentially as described (Latham *et al.*, 1990). Equimolar amounts of transcripts were annealed in TE [10 mM Tris–HCl (pH 7.6), 1 mM EDTA (pH 8.0)] by mixing the two RNAs, heating to 92°C for 5 min and then slowly cooling to room temperature. These RNA molecules were stored at –20°C and used for EM analysis.

Cloning of extended L-21 Sca I ribozyme templates

DNA segments encoding either the 5′ half or 3′ half of the extension plus appropriate portions of the L-21 ribozyme were generated by 100 µl PCRs containing 10 mM Tris–HCl, pH 8.3, 4 mM $MgCl_2$, 50 mM KCl, 0.15 mM of each dNTP and 5 U of *Taq* DNA polymerase (Boehringer Mannheim), using 10–15 nM of either pTZ L-21 (Grosshans and Cech, 1991) or pTZ L-21P8*Bam*H (TGTAT at L8 was changed to GGATCC to introduce a *Bam*HI site) as template and 20 µM each of appropriate primer pairs. The *Bam*HI site introduced into P6b and *cis*-P1 + P6b was the result of our initial attempt to introduce extensions as one palindromic sequence into the plasmid. The ribozyme with this *Bam*HI site in L8 shows activity indistinguishable from the wt ribozyme (data not shown). The PCR was first heated to 96°C for 2 min and *Taq* polymerase was added to start the reaction. 30 cycles (94°C 30 s, 50°C 45 s and 72°C 1 min) were followed by 72°C 10 min. The following DNA primers were used: PCR INT 5′-GAG CGG ATA ACA ATT TCA CAC A-3′, PCR END 5′-AGT GCC AAG CTT GTG ACG-3′, P1 EXT1 5′-GTA CCG GGA TCC AAT TAA TAC GAC TCA CTA TAG GCC CTC TAA AGG TAA ATA TTG CTA TTT TGC ACT TTA TGC GGA CAC TTC CTA CAG GTA GAA TTC GCG GTA-3′, PCR P1a 5′-GTA CCG GGA TCC AAT TAA-3′, PCR P1b 5′-TAC CGC GAA TTC TAC CTG-3′, P1 EXT2 5′-GTA CCG GAA TTC TCT ACC TGT AGG AAG TGT CCG CAT AAA GTG CAA AAT AGC AAT ATT TAC CTT TGG AGG GAA AAG TTA TCA GGC ATG CA-3′, P2.1 EXT1 5′-GCG GGA TCC CCG GGT CCA TCG CAA CTG GGA TTG AAA CCA GCA GCC CAT GCG TTA GCG GCG GTC ATC TAT TGG TTT AAA GAC TAG CTA CC-3′, P2.1 EXT2 5′-CGG GAT CCC CGG GAG GTC CAT CGC AAC TGG GAT TGA AAC CAG CAG CCC ATG CGT TAG CGG CGG TCA TCT ATC GGT TTA AAA GGC AAG ACC GTC A-3′, P2.1 EXT3 5′-CGG GAT CCC CGG GAG GTC CAT CGC AAC TGG GAT TGA AAC CAG CAG CCC ATC CGT-3′, P6 EXT1 5′-CTA CGC TCT AGA TGA GGC TTG TCA TTC TAC ATT CAT CAT AGG ATT ACG GAA AGA TGA TAT TTT AGT TAA GGT GAG GAG GCA TAA TAC AGA TCT GTT GAC TTA GGA CTT G-3′, P6 EXT2 5′-CTA CGC TCT AGA GGC TTG TCA TTC TAC ATT CAT CAT AGG ATT ACG GAA AGA TGA TAT TTT AGT TAA GGT GAG GAG GCA TAA TAC AGA TCT GTT GAT ATG GAT GCA GTT CA-3′, P8 EXT1 5′-CTA CGC CTC GAG TCG ATT ATT ACC TTC ATC ACT TCA TCG CGA TGC GTA TTT GGG CGC TTT TCC TAA GTA CCG TTC AAC CGA TGT ATC GGA TCC TCT TCC CCG ACC GAC ATT TA-3′, P8 EXT2 5′-CTA CGC CTC GAG ATT ATT ACC TTC ATC ACT TCA TCG CGA TGC GTA TTT GGG CGC TTT TCC TAA GTA CCG TTC AAC CGA TGT ATC GGA TCC TCT TCT CAT AAG ATA TA-3′, P8 EXT3 5′-GCA CGC GTC GAC ATT ATT ACC TTC ATC ACT TCA TCG CGA TGC GTA TTT GGG CGC TTT TCC TAA GTA CCG TTC AAC-3′, P9.2 EXT1 5′-CGG GGT ACC ACC GTA CGG TCC TGT CCG ACT CGA ATC TTG GCT GAA CGG TAC TCG CGA CAT CGC ATA CAA ATT AGT

TCC CAG CGG CT-3′, PCR P9.2a 5′-CGG GGT ACC CAC CGT ACG-3′, PCR P9.2b 5′-TCG ATG CGC TCG AGT ACT-3′, P9.2 EXT2 5′-CGG GGT ACC CAC CGT ACG GTC CTG TCC GAC TCG AAT CTT GGC TGA ACG GTA CTC GCG ACA TCG TAT ATT GAT TAG TTT TGG AGT ACT CGA GCG CAT CGA-3′ (for long primers, annealing regions are underlined; see Figure 3A for relative location and orientation of primers). PCR products were digested with appropriate restriction enzymes (NEB), gel-purified and ligated into either pUC19, pTZ18U (NEB) or pBluescript SK+ (Stratagene) using T4 DNA ligase (NEB). (Complete details of the plasmid construction are available from T.M.Nakamura and T.R.Cech upon request.) The extended sequence and the ribozyme portions of resulting plasmids were sequenced from both directions by Sanger's method using Sequenase and following the manufacturer's instructions (USB). Once the sequence was confirmed, large scale plasmid preparation was done using QIAGEN plasmid Maxi Kit.

Extended ribozyme RNA preparation

Plasmids encoding various parts of the ribozyme and the extensions were digested with appropriate restriction enzymes and ligated by T4 DNA ligase. Ligated DNAs were then amplified by PCR with the EcoR-T7 primer (5′-CCG GAA TTC AAT TAA TAC GAC TCA CTA TAG-3′) and the Sca-END primer (5′-ACT CCA AAA CTA ATC AAT ATA CTT TCG CAT-3′) using conditions similar to that described in the previous section, except that an annealing temperature was varied from 50°C to 60°C and cycle numbers were also varied depending on the construct. PCR products were run on 2–4% NuSieve GTG agarose (FMC BioProducts) and purified by QIAquick gel extraction kit (QIAGEN). Ribozymes were prepared by transcribing these DNA templates with phage T7 RNA polymerase with purification by gel electrophoresis (Latham *et al.*, 1990). Ribozyme concentration was determined spectrophotometrically.

Kinetics studies

Single-turnover reactions were performed with <5 nM of 5′ end-labeled RNA substrate (5′-CCCUCUAAAAA-3′) and excess (≥10-fold) ribozyme. Reactions were carried out at 50°C in 50 mM 2-(*N*-morpholino)ethanesulfonic acid (MES), sodium salt, pH 7.0 (pH was determined at 25°C). Ribozymes were preincubated at 50°C in the presence of buffer and 10 mM Mg^{2+} for 20 min to allow formation of a single active folded species (≥90%) of ribozyme (Herschlag and Cech, 1990; McConnell *et al.*, 1993). For $(k_{cat}/K_m)^S$ measurements, 5 nM ribozyme and 2 mM guanosine (final concentration) were used, and the reaction was started by addition of a trace amount of labeled substrate. For $(k_{cat}/K_m)^G$ measurements, 100 nM ribozyme (final concentration) was used, and the reaction was started by simultaneous addition of labeled substrate and 1 μM guanosine (final concentration). Typically, eight portions (2 μl each) were removed from a reaction mixture (20 μl) and quenched with 2 μl of stop buffer containing 80% formamide, 50 mM EDTA, 0.1% bromophenol blue, 0.1% xylene cyanol and 2 mM Tris borate, pH 7.5. Products were run on 20% polyacrylamide (acrylamide:bis-acrylamide, 29:1)–7 M urea gels in 1× TBE and quantitated by PhosphorImager (Molecular Dynamics) scanning. The fraction RNA substrate remaining (y) was plotted as a function of time, and k_{obs} (min^{-1}) was determined by fitting to $y = (1 - b)e^{-k_{obs}t} + b$, where b = fraction of substrate that was unreactive after long incubation; $(k_{cat}/K_m)^S$ was calculated as k_{obs}/5 nM, where 5 nM was the concentration of ribozyme, and $(k_{cat}/K_m)^G$ was calculated as k_{obs}/1 μM, where 1 μM was the concentration of guanosine.

Electron microscopy

Methods for preparing RNA samples for direct mounting have been described (Wang *et al.*, 1994) and were used with some modifications. RNA samples (18 nM RNA ± 190 nM product oligonucleotide) were incubated at 50°C for 10 min in 35 mM Tris–HCl (pH 7.5) in the presence of 70 mM $MgCl_2$. [The $MgCl_2$ is washed away during the sample preparation, and our previous study had shown that a high initial $MgCl_2$ concentration is necessary to stabilize the tertiary structure of the RNA, which only requires ~2 mM $MgCl_2$ in solution (Celander and Cech, 1991).] The samples were further incubated at 42°C for 5 min, then mixed with spermidine hydrochloride (final concentration 250 μM), and adsorbed to glow-charged copper mesh grids covered by thin carbon films for 30 s at room temperature. The grids were washed with 35 mM Tris buffer containing 70 mM Mg^{2+} for 1 min, dehydrated through a graded ethanol series (50%, 75%, 100%, 5 min each), air-dried and rotary shadowcast with tungsten. Micrographs were taken on a Philips EM400 TLG electron microscope. A Cohu CCD camera attached to a Macintosh computer programmed with the NIH IMAGE software was used to measure angles and to form montages of the images.

Acknowledgements

We thank Paul Hagerman for gifts of pGJ122A9 and pGJ122B11 plasmids prior to publication, Jennifer Doudna and Bruce Sullenger for helpful discussions on the construction of extended ribozymes, Cheryl Grosshans for synthesis of PCR primers and Alice Sirimarco for manuscript preparation. This work was supported by grants from the NIH to T.R.Cech (GM28039) and to J.D.Griffith (GM31819) and from the American Cancer Society to J.D.Griffith (NP583). T.R.Cech is an Investigator of the Howard Hughes Medical Institute and an American Cancer Society Professor. We thank the W.M.Keck Foundation for their generous support of RNA research at the University of Colorado at Boulder.

References

Amiri,K.M.A. and Hagerman,P.J. (1994) Global conformation of a self-cleaving hammerhead RNA. *Biochemistry*, **33**, 13172–13177.

Bassi,G.S., Møllegaard,N.-E., Murchie,A.I.H., von Kitzing,E. and Lilley,D.M.J. (1995) Ionic interactions and the global conformations of the hammerhead ribozyme. *Nature Struc. Biol.* **2**, 45–55.

Bhattacharyya,A., Murchie,A.I.H. and Lilley,D.M.J. (1990) RNA bulges and the helical periodicity of double-stranded RNA. *Nature*, **343**, 484–487.

Brimacombe,R., Atmadja,J., Stiege,W. and Schuler,D. (1988) A detailed model of the three-dimensional structure of *Escherichia coli* 16S ribosomal RNA *in situ* in the 30 S subunit. *J. Mol. Biol.*, **199**, 115–136.

Cech,T.R. (1990) Self-splicing of group I introns. *Annu. Rev. Biochem.*, **59**, 543–568.

Cech,T.R. (1993) Structure and mechanism of the large catalytic RNAs: Group I and group II introns and ribonuclease P. In Gesteland,R.F. and Atkins,J.F. (eds), *The RNA World.* Cold Spring Harbor Laboratory Press, Cold Spring Harbor, NY, pp. 239–269.

Cech,T.R., Herschlag,D., Piccirilli,J.A. and Pyle,A.M. (1992) RNA catalysis by a group I ribozyme. *J. Biol. Chem.*, **267**, 17479–17482.

Cech,T.R., Damberger,S.H. and Gutell,R.R. (1994) Representation of the secondary and tertiary structure of group I introns. *Nature Struct. Biol.*, **1**, 273–280.

Celander,D.W. and Cech,T.R. (1991) Visualizing the higher order folding of a catalytic RNA molecule. *Science*, **251**, 401–407.

Collins,J. (1980) Instability of palindromic DNA in *Escherichia coli*. *Cold Spring Harbor Symp. Quant. Biol.*, **45**, 409–416.

Damberger,S.H. and Gutell,R.R. (1994) A comparative database of group I intron structures. *Nucleic Acids Res.*, **22**, 3508–3510.

Downs,W.D. and Cech,T.R. (1990) An ultraviolet-inducible adenosine–adenosine crosslink reflects the catalytic structure of the *Tetrahymena* ribozyme. *Biochemistry*, **29**, 5605–5613.

Friederich,M.W., Gast,F.-U., Vacano,E. and Hagerman,P.J. (1995) Determination of the angle between the anticodon and aminoacyl acceptor stems of yeast phenylalanyl tRNA in solution. *Proc. Natl Acad. Sci. USA*, **92**, 4803–4807.

Gold,L. *et al.* (1993) RNA: The shape of things to come. In Gesteland,R.F. and Atkins,J.F. (eds), *The RNA World.* Cold Spring Harbor Laboratory Press, Cold Spring Harbor, NY, pp. 497–509.

Grosshans,C.A. and Cech,T.R. (1991) A hammerhead ribozyme allows synthesis of a new form of the *Tetrahymena* ribozyme homogeneous in length with a 3′ end blocked for transesterification. *Nucleic Acids Res.*, **19**, 3875–3880.

Harris,M.E., Nolan,J.M., Malhotra,A., Brown, J.W., Harvey,S.C. and Pace, N.R. (1994) Use of photoaffinity crosslinking and molecular modeling to analyze the global architecture of ribonuclease P RNA. *EMBO J.*, **13**, 3953–3963.

Herschlag,D. and Cech,T.R. (1990) Catalysis of RNA cleavage by the *Tetrahymena thermophila* ribozyme. 1. Kinetic description of the reaction of an RNA substrate complementary to the active site. *Biochemistry*, **29**, 10159–10171.

Kim,S.-H., Suddath,F.L., Quigley,G.J., McPherson,A., Sussman,J.L., Wang,A., Seeman,N. and Rich,A. (1974) Three-dimensional tertiary structure of yeast phenylalanine transfer RNA. *Science*, **185**, 435–440.

Latham,J.A. and Cech,T.R. (1989) Defining the inside and outside of a catalytic RNA molecule. *Science*, **245**, 276–282.

Latham,J.A., Zaug,A.J. and Cech,T.R. (1990) Self-splicing and enzymatic cleavage of RNA by a group I intervening sequence. *Methods Enzymol.*, **181**, 558–569.
Lilley,D.M. (1981) *In vivo* consequences of plasmid topology. *Nature*, **292**, 380–382.
Malhotra,A. and Harvey,S.C. (1994) A quantitative model of the *Escherichia coli* 16S RNA in the 30S ribosomal subunit. *J. Mol. Biol.*, **240**, 308–340.
McConnell,T.S., Cech,T.R. and Herschlag,D. (1993) Guanosine binding to the *Tetrahymena* ribozyme: thermodynamic coupling with oligonucleotide binding. *Proc. Natl Acad. Sci. USA*, **90**, 8362–8366.
Michel,F. and Dujon,B. (1983) Conservation of RNA secondary structures in two intron families including mitochondrial-, chloroplast- and nuclear-encoded members. *EMBO J.*, **2**, 33–38.
Michel,F. and Westhof,E. (1990) Modeling of the three-dimensional architecture of group I catalytic introns based on comparative sequence analysis. *J. Mol. Biol.*, **216**, 585–610.
Moazed,D. and Noller,H.F. (1989) Interaction of tRNA with 23S rRNA in the ribosomal A, P, and E sites. *Cell*, **57**, 585–597.
Murphy,F.L. and Cech,T.R. (1993) An independently folding domain of RNA tertiary structure within the *Tetrahymena* ribozyme. *Biochemistry*, **32**, 5291–5300.
Murphy,F.L. and Cech,T.R. (1994) GAAA tetraloop and conserved bulge stabilize tertiary structure of a group I intron domain. *J. Mol. Biol.* **236**, 49–63.
Murphy,F.L., Wang,Y.-H., Griffith,J.D. and Cech,T.R. (1994) Coaxially stacked RNA helices in the catalytic center of the *Tetrahymena* ribozyme. *Science*, **265**, 1709–1712.
Pley,H.W., Flaherty,K.M. and McKay,D.B. (1994) Three-dimensional structure of a hammerhead ribozyme. *Nature*, **372**, 68–74.
Price,J.V., Kieft,G.L., Kent,J.R., Sievers,E.L. and Cech,T.R. (1985) Sequence requirements for self-splicing of the *Tetrahymena thermophila* pre-ribosomal RNA. *Nucleic Acids Res.*, **13**, 1871–1889.
Pyle,A.M., Murphy,F.L. and Cech,T.R. (1992) RNA substrate binding site in the catalytic core of the *Tetrahymena* ribozyme. *Nature*, **358**, 123–128.
Robertus,J.D., Ladner,J.E., Finch,J.T., Rhodes,D., Brown,R.S., Clark,B.F. and Klug,A. (1974) Structure of yeast phenylalanine tRNA at 3Å resolution. *Nature*, **250**, 546–551.
Shen,Z. and Hagerman,P.J. (1994) Conformation of the central, three-helix junction of the 5 S ribosomal RNA of *Sulfolobus acidocaldarius*. *J. Mol. Biol.*, **241**, 415–430.
Stern,S., Weiser,B. and Noller,H.F. (1988) Model for the three-dimensional folding of 16 S ribosomal RNA. *J. Mol. Biol.*, **204**, 448–481.
Szostak,J.W. (1986) Enzymatic activity of the conserved core of a group I self-splicing intron. *Nature*, **322**, 83–86.
Tanner,N.K., Schaff,S., Thill,G., Petit-Koskas,E., Crain-Denoyelle,A.M. and Westhof,E. (1994) A three-dimensional model of hepatitis delta virus ribozyme based on biochemical and mutational analyses. *Curr. Biol.*, **4**, 488–498.
Tuschl,T., Gohlke,C., Jovin,J.M., Westhof,E. and Eckstein,F. (1994) A three-dimensional model for the hammerhead ribozyme based on fluorescence measurements. *Science*, **266**, 785–789.
Wang,J.-F. and Cech,T.R. (1992) Tertiary structure around the guanosine-binding site of the *Tetrahymena* ribozyme. *Science*, **256**, 526–529.
Wang,J.-F., Downs,W.D. and Cech,T.R. (1993) Movement of the guide sequence during RNA catalysis by a group I ribozyme. *Science*, **260**, 504–508.
Wang,Y.-H., Murphy,F.L., Cech,T.R. and Griffith,J.D. (1994) Visualization of a tertiary structural domain of the *Tetrahymena* group I intron by electron microscopy. *J. Mol. Biol.*, **236**, 65–71.
Waring,R.B., Scazzocchio,C., Brown,T.A. and Davies,R.W. (1983) Close relationship between certain nuclear and mitochondrial introns. *J. Mol. Biol.*, **167**, 595–605.
Westhof,E. and Altman,S. (1994) Three-dimensional working model of M1 RNA, the catalytic RNA subunit of ribonuclease P from *Escherichia coli*. *Proc. Natl Acad. Sci. USA*, **91**, 5133–5137.
Westhof,E., Romby,P., Romaniuk,P.J., Ebel,J.-P., Ehresmann,C. and Ehresmann,B. (1989) Computer modeling from solution data of spinach chloroplast and of *Xenopus laevis* somatic and oocyte 5 S rRNAs. *J. Mol. Biol.*, **184**, 417–431.
Woese,C.R. and Pace,N.R. (1993) Probing RNA structure, function, and history by comparative analysis. In Gesteland,R.F. and Atkins,J.F. (eds), *The RNA World.* Cold Spring Harbor Laboratory Press, Cold Spring Harbor, NY, pp. 91–117.
Wyatt,J.R. and Tinoco,I.,Jr. (1993) RNA structural elements and RNA function. In Gesteland,R.F. and Atkins,J.F. (eds) *The RNA World.* Cold Spring Harbor Laboratory Press, Cold Spring Harbor, NY, pp. 465–496.
Zaug,A.J., Been,M.D. and Cech,T.R. (1986) The *Tetrahymena* ribozyme acts like an RNA restriction endonuclease. *Nature*, **324**, 429–433.

Received on June 13, 1995; revised on July 11, 1995